Coexistence of magnetic and dielectric glassy states in alternating kagome and triangular lattice $LuBaCo_4O_7$ cobaltite

C. Dhanasekhar,[1,2,3,*] D. Chandrasekhar Kakarla,[2] Archana Kumari,[4] Monika Jawale,[1] Ronit Hindoddikar,[5] Ajay Tiwari,[2] Patri Tirupathi,[6] Cang Ting Lai,[2] Mitch M. C. Chou,[3] A. Venimadhav,[5] H. D. Yang,[2,3,†] Praveen Chaddah,[7,‡] and A. V. Mahajan[1,§]

[1]*Department of Physics, Indian Institute of Technology Bombay, Mumbai 400076, India*
[2]*Department of Physics, National Sun Yat-sen University, Kaohsiung 80424, Taiwan*
[3]*Center of Crystal Research, National Sun Yat-sen University, Kaohsiung 80424, Taiwan*
[4]*Department of Physics, Indian Institute of Science, Bengaluru 560012, India*
[5]*Cryogenic Enginerring Centre, Indian Institute of Technology, Kharagpur 721302, India*
[6]*University Department of Physics, Tilka Manjhi Bhagalpur University, Bhagalpur 812007, India*
[7]*UGC-DAE Consortium for Scientific Research, Khandwa Road, Indore 452001, India*

(Received 23 September 2024; accepted 28 April 2025; published 21 May 2025)

To date, the alternating kagome and triangular lattice cobaltites, i.e., $RBaCo_4O_7$ (R = Ca, Y, and rare-earth), have been well studied due to their large structural distortions, anisotropic exchange interactions, chiral spin liquid states, and giant multiferroic properties. Here, we report the coexistence of magnetic and dielectric glassy states in $LuBaCo_4O_7$ cobaltite below 50 K. AC magnetization studies show an absence of conventional spin freezing phenomena. The cooling and heating in unequal field (CHUF), thermal cycling of magnetization, and time-dependent magnetization studies at the low temperature (T) show the presence of the magnetic glassy state. The dielectric constant (ϵ') exhibits a strong frequency-independent response at 45 K and dipolar glassy features below 20 K. The nonequilibrium magnetic glassy dynamics and dipolar glassy state at low T arises from the kinetic arrest of monoclinic (Cc) and orthorhombic ($Pbn2_1$) phases. From the dielectric probe, we are able to clearly distinguish the kinetically arrested phases at low T, whereas the bulk magnetization studies are unable to do so, as the arrested phases have low magnetic moments.

DOI: 10.1103/PhysRevB.111.174438

I. INTRODUCTION

$RBaCo_4O_7$ (R = Ca, Y, In, and rare-earth) oxides, known as the R-114 cobaltites family, act as a model system for studying the interplay between structural, magnetic, thermal, and electrical properties [1–9]. The trigonal structural framework of R-114 consists of alternating two-dimensional kagome and triangular layers, with cobalt ions sitting at the centers of corner-sharing oxygen tetrahedra. In R-114 oxides, the cobalt ions are in mixed Co^{2+} and Co^{3+} states to maintain a charge balance and distributed among the two independent sites, located in the kagome and triangular layers. For trivalent R ions (such as In, Y, or a rare-earth element) in R-114 oxides, the average Co oxidation state is expected to be 2.25+, with a Co^{2+}/Co^{3+} ratio of 3:1 [10]. The R-114 cobaltites undergo a first-order structural phase transition from trigonal $P31c$ to orthorhombic $Pbn2_1$, where the transition temperature (T) is denoted as T_{S1}. For large R ions, T_{S1} occurs slightly above room T and decreases to about 100 K with decreasing size of the R ion [1,3,4,11].

At low T (T < 100 K), the R-114 cobaltites display diverse magnetic properties, and the magnetic ground state is significantly influenced by the R cation [4]. For example, $CaBaCo_4O_7$ (CBCO) exhibits clear ferrimagnetic order below 70 K [12–14], $InBaCo_4O_7$ (IBCO) exhibits spin-glass-like freezing [15], spin glass along with short-range magnetic correlations, and also Griffiths phase in $DyBaCo_4O_{7\pm\delta}$ [16,17] spin-liquid-like properties along with long-range antiferromagnetic (AFM) ordering (T_N) in $YBaCo_4O_7$ (YBCO) [18,19]. The doping of Fe at Co sites in YBCO leads to the chiral spin liquid ground state [20]. $TbBaCo_4O_7$ shows coexisting long-range and short-range magnetic phases and converted to long range under an applied field [21,22]. Extensive doping studies have been carried out in CBCO at Ca and Co sites, which suppress the long-range ferrimagnetic order and induce the cluster or spin glass phases [23,24].

In previous studies, it was reported that $LuBaCo_4O_7$ (LBCO) shows two successive first-order phase transitions, i.e., at T = 160 K; from the trigonal $P31c$ phase to the monoclinic Cc phase and at $T \approx 110$ K from the monoclinic Cc phase to the orthorhombic $Pbn2_1$ phase [7,25]. The $P31c$ to Cc phase transition was clearly evident from electrical resistivity and specific heat measurements. Conversely, the Cc to $Pbn2_1$ phase transition features were shown in specific heat and magnetization (M) studies, and at this transition, M shows a large thermal hysteresis. Among R-114 cobaltites,

*Contact author: dsekhar21iitb@gmail.com
†Contact author: yang@mail.nsysu.edu.tw
‡Contact author: chaddah.praveen@gmail.com
§Contact author: mahajan@phy.iitb.ac.in

the monoclinic Cc phase is unique to LBCO and is not observed/reported in other materials of this family. At low T, M studies observed a significant peak at 48 K, which is not related to any long-range magnetic order but is assigned to the representation of the metastable supercooled phase. Extensive synchrotron and neutron powder diffraction studies at low T reported the coexistence of Cc and $Pbn2_1$ phases and their phase fraction is strongly dependent on the cooling rate [7]. Slow cooling rates ($\frac{dT}{dt} < 3$ K/min) resulted in coexisting $Pbn2_1$ and Cc phases, with varying fractions dependent on the cooling rate. Fast cooling ($\frac{dT}{dt} \geqslant 3.5$ K/min) suppressed the low-T, $Pbn2_1$ phase and allowed the high-T, $P31c$ phase to convert to a metastable Cc phase below 160 K, which is expected to be stable down to 2 K. Further, neutron powder diffraction studies showed absence of long-range magnetic ordering in Lu-114 down to 2 K, and additionally showed broad diffuse magnetic scattering intensities at low T, indicating short-range magnetic correlations at low T. However, single-crystal neutron diffraction studies on LBCO at low T showed a commensurate- and incommensurate-like modulation of the cobalt moments on the kagome and triangular lattices [25,26].

Although neutron studies in LBCO revealed short-range magnetic correlations and commensurate- or incommensurate-like phases at low T, bulk M measurements showed a significant peak at 48 K and broad thermal hysteresis between 70 K and 110 K. This observation motivated us to conduct detailed M studies to investigate the presence of glasslike features in LBCO at low T. If there are glassy features, the nature of the glassy state, and whether the glassy state is associated with first-order phase transitions and is influenced by the different phases. To answer these questions, we have examined the magnetic ground state of LBCO using various magnetic measurement protocols. Our results show that the first-order structural phase transitions in LBCO are kinetically arrested at low T and form a nonequilibrium magnetic state, i.e., a magnetic glass. Furthermore, due to the noncentrosymmetric crystal structure and significant structural distortions, the R-114 cobaltites are anticipated to show strong correlations among their structural, magnetic, and dielectric properties [2,4,6,9]. In this family of materials, it is reported that CBCO cobaltite shows large structural distortions that stabilize the polar orthorhombic $Pbn2_1$ phase up to 4 K and these distortions stabilize the long-range ferrimagnetic ground state (FiM) up to 70 K. The large structural distortions, together with long-range FiM order, further drive the giant spin-order-driven electric polarization in CBCO below 70 K [6,9]. In this study, we demonstrate the strong correlations among these properties, even in the absence of the large structural distortions and long-range magnetic ground state. Detailed dielectric measurements demonstrate structural phase transitions strongly coupled with dielectric properties and show a dipolar glassy state at low T, which arises from the supercooled and kinetically arrested metastable phase, that is, monoclinic Cc.

II. EXPERIMENTAL DETAILS

The $LuBaCo_4O_7$ (LBCO) sample was prepared by a solid-state reaction method. The starting materials of Lu_2O_3 (99.995%, Alfa Aesar), $BaCO_3$ (99.9%, Alfa Aesar), and Co_3O_4(99.7%, Alfa Aesar) were mixed in the appropriate ratio. The homogeneous powder was placed in a platinum crucible with a lid and heated in air at 900 °C for 12 h and at 1150 °C for 48 h with intermediate grindings. To stabilize the 114 phase, the sample was directly quenched in air from 1150 °C to room temperature, which is necessary, similar to the other cobalt compounds in this family [14,23,24]. The room-temperature powder x-ray diffraction (XRD) on LBCO samples was performed using a PANalytical X′pert PRO diffractometer equipped with Cu-$K\alpha$ radiation radiation ($\lambda = 1.54182$ Å). The experimental XRD data is analyzed through the Rietveld refinement method using FULLPROF Suite software. All the dc and ac magnetic measurements were performed using a Magnetic Property Measurement System (MPMS, SQUID VSM), Quantum Design, USA. All the dc magnetization measurements were performed during both cooling and heating at rates of 3 K/min, and the ac magnetization measurements were performed under heating rates of 1 K/min. Temperature-dependent dielectric ($\epsilon'(T)$) measurements were performed using an LCR meter (Agilent E4980A). All the dielectric and pyroelectric current measurements were conducted using the Janis cryogenic and Quantum Design MPMS systems supplemented by a homemade multifunctional probe attached to the MPMS. The pyroelectric current (I_p) was measured using a Keithley 6517A electrometer under conventional electric poling and bias poling electric field methods during warming temperature cycles [13,27,28]. A pellet of area 48.9 mm^2 and thickness of 0.3 mm was used for the dielectric and pyroelectric current measurements. The $\epsilon'(T)$ measurements are performed under an ac excitation field of 1 V with silver paint applied to both sides of the sample to act as the electrodes. The cooling- and heating-dependent $\epsilon'(T)$ measurements were performed under 2 K/min and 1 K/min rates, and these temperature ramping conditions are specified in the relevant main text. Resistivity measurements were performed using standard four-probe geometry in a Janis cryogenic PPMS system with a Keithley 2400 source meter.

III. RESULTS AND DISCUSSION

A. Room-temperature x-ray diffraction studies

The room-temperature x-ray diffraction (XRD) patterns of the $LuBaCo_4O_7$ sample, along with Rietveld refinement, are shown in Fig. 1. Rietveld analysis confirms that LBCO belongs to the trigonal $P31c$ space group with the lattice parameters $a = b = 6.26350$ (03) Å, $c = 10.22467$ (10) Å, and $V = 347.388$ (4) $Å^3$, respectively. The obtained lattice parameters are within the range of reported values [7] and the refinement agreement factors are given in the inset of Fig. 1.

B. dc magnetization studies

The T-dependent magnetization (M) of LBCO was measured under a magnetic field (H) of 1 T under zero-field-cooled (ZFC), field-cooled cooling (FCC), and field-cooled warming (FCW) protocols, as shown in Fig. 2(a). The M vs T curves curves show several anomalies with decreasing T. All anomalies match well with previous polycrystalline and

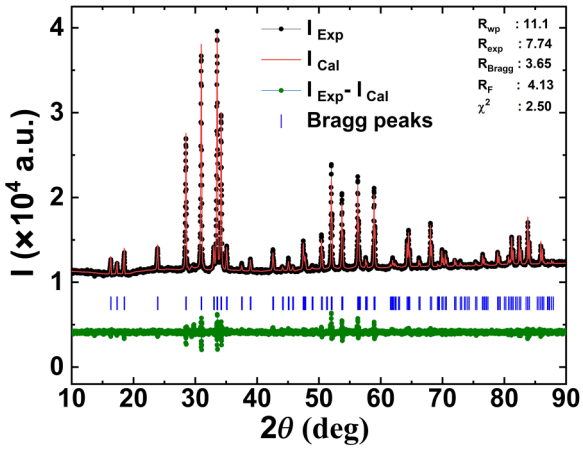

FIG. 1. Room-temperature powder x-ray diffraction data of the $LuBaCo_4O_7$ sample along with the corresponding Rietveld refinement model.

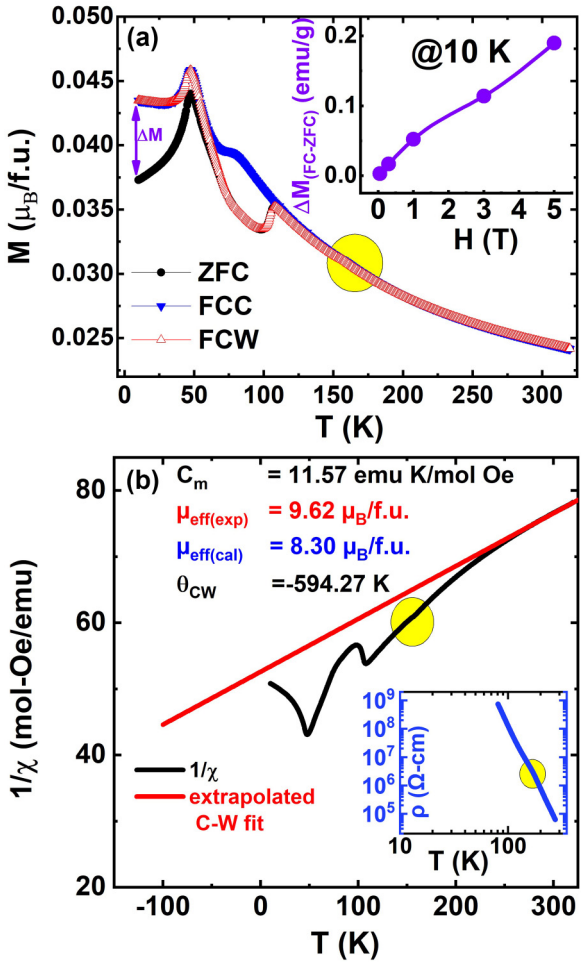

FIG. 2. (a) shows the M vs T curves of the $LuBaCo_4O_7$ sample measured using ZFC, FCC, and FCW protocols under $H = 1$ T. (b) shows the $1/\chi$ vs T data along with the extrapolated C-W fitting. The inset of (a) shows the ΔM vs H measured at 10 K and inset of (b) shows the ρ vs T in log-log scale.

single-crystal studies of LBCO [7,25]. With decreasing T, the M vs T curves show a small kink at 160 K [yellow circle in Figs. 2(a) and 2(b)], and this transition was not observed in previous M studies. The ρ vs T measurements show a slope change at $T = 160$ K [inset of Fig. 2(b)], similar to earlier resistivity measurements [7]. However, specific heat and neutron scattering studies showed changes at this T, owing to the structural transition from trigonal P 31c to monoclinic Cc. Further, as T decreases, the M vs T [ZFC/FCW (heating) and FCC (cooling) protocols] show a large thermal hysteresis in the range of 60–110 K (∼50 K). At low T, the M vs T curves show a clear peak at 48 K and strong irreversibility between the ZFC and FCC/FCW curves below 48 K. The difference between the ZFC and FCC magnetization, i.e., ΔM ($M_{FC} - M_{ZFC}$) at 10 K increases with H and is shown in the inset of Fig. 2(a). The high-T magnetic susceptibility data was fitted with the Curie-Weiss (CW) law

$$\chi = \frac{C_m}{T - \theta_{CW}}, \tag{1}$$

where C_m denotes the molar Curie constant and θ_{CW} denotes the C-W temperature. The fitting gives a $\theta_{CW} = -594.27$ K and $\mu_{eff} = 9.62\,\mu_B$/f.u.. The fitting is shown in Fig. 2(b), which clearly deviates below 220 K, Such behavior was also observed in other compounds in this family [23,29,30], where the deviation is caused by the short-range magnetic correlations associated with the kagome and triangular lattice arrangements of Co ions together with the structural phase transitions at high T. The high spin state of Co^{2+} ($s = \frac{3}{2}$) and Co^{3+} ($s = 2$) ions in an tetrahedral crystal field gives an effective spin-only moment as $\mu_{cal} = \sqrt{3\mu^2_{Co^{2+}} + \mu^2_{Co^{3+}}} = 8.30\,\frac{\mu_B}{\text{f.u.}}$, where $\mu_{Co^{2+}} = 3.87\ \mu_B$ and $\mu_{Co^{3+}} = 4.90\ \mu_B$, respectively. The calculated moments from the C-W fitting are higher than the spin values, suggesting that the orbital moments of Co^{3+} and Co^{2+} ions may not be quenched.

C. ac magnetization studies

Figures 3(a) and 3(c) show the real (χ') and imaginary (χ'') components of ac magnetization, measured for the different frequencies of LBCO in the T interval of 10–120 K. For all frequencies, χ' shows a sharp and frequency-independent maximum close to 48 K and χ'' is approximately a straight line. The sharp peak of χ' at 48 K matches with the dc M peak observed at this T. Further, a frequency-independent and steplike peak was observed near 110 K, where the first-order structural phase transition is observed. Further, we also measured $\chi'(T)$ with (3 h) and without waiting at $T = 22$ K for the frequency of 73 Hz and results are shown in Fig. 3(b). The $\chi'_{t=3h}$ and $\chi'_{t=0h}$ (ref) both were measured while heating the sample with a heating rate of 1 K/min. In these measurements, the main difference is in the cooling of the sample. In case $\chi'_{t=3h}$, the temperature is stopped at 22 K for 3 h (waiting time), whereas in $\chi'_{t=0h}$ (ref), the T was not stopped at 22 K. Interestingly, the magnitude of $\chi'_{t=3h}$ is greater than $\chi'_{t=0h}$ (ref), and both the curves overlap above 70 K [Fig. 3(b)]. In conventional spin glasses, the difference in $\Delta\chi'$ [$\chi'_{t=3h} - \chi'_{t=0h}$ (ref)] would be expected to shows diplike features at the waiting temperature [31–33]. The $\Delta\chi'$ does not show any such features at 22 K, instead, it shows a

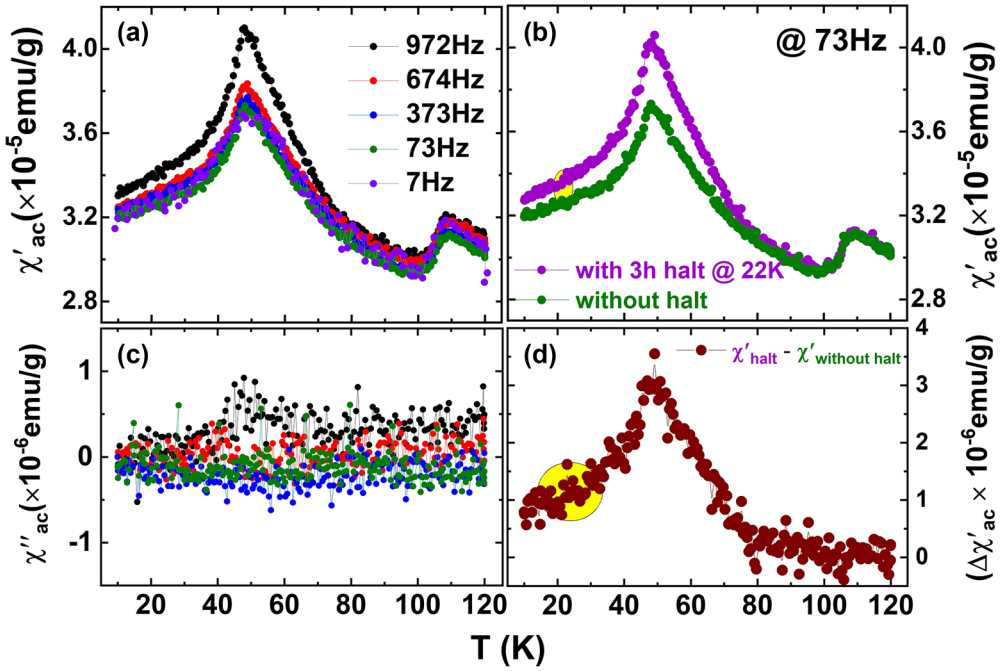

FIG. 3. (a) and (c) show the temperature- and frequency-dependent real (χ') and imaginary (χ'') components of ac magnetization of the $LuBaCo_4O_7$ sample. (b) and (d) show the χ' low-frequency susceptibility data obtained with the standard experimental approach for observing the memory effect.

clear peak at 48 K. The absence of the $\triangle\chi'$ dips at the waiting temperature has also been reported in layered $EuBaCo_2O_{5+\delta}$ ($\delta = 0.47$) cobaltite [34], where conventional spin freezing features also absent. Such, χ', χ'', and $\triangle\ \chi'$ features rule out the conventional spin glass behavior in the title compound.

D. Kinetic arrest and metastability

The above ac magnetization results show the absence of the conventional spin-glass behavior and the dc magnetization studies reveal that various anomalies are strongly coupled with structural changes, the FCC and FCW curves show a strong thermal hysteresis. Previous studies predicted that the peak at 48 K is associated with the metastable supercooled phase [7]. However, a detailed understanding of this peak and the nature of the supercooled phase is missing. Here, we used different magnetic measurement protocols, including cooling and heating in unequal fields (CHUF) [35,36], time-dependent magnetization and field-cooled isothermal magnetization studies to shed light on the low-T magnetic phase. CHUF measurements have been extensively used to unravel the phase coexistence through the response of materials to external perturbations [37–42].

Following the CHUF1 protocol (i.e., cooling in unequal fields and heating in same field), the LBCO sample was cooled from 250–10 K under various cooling magnetic fields (H_{cool}), i.e., 0, 0.05, 0.5, 1, 2, 3, and 5 T, respectively. At 10 K the H_{cool} was changed to the measuring magnetic field (H_{meas}) of 1 T and the obtained results are shown in Fig. 4. For $T > 70$ K, the M behavior of LBCO under CHUF1 remains the same irrespective of H_{cool}. For $T < 70$ K, the M curves show a dispersion, which increases with decreasing T. The peak position at 48 K is independent of H_{cool}, the behavior of the M vs T curves changes with H_{cool} for $T < 48$ K. For $H_{cool} < H_{meas}$, M increases from 10–48 K, for the $H_{cool} = H_{meas}$, the M is almost constant and for the $H_{cool} > H_{meas}$, M decreases. We also used another CHUF protocol, CHUF2 (i.e., cooling in the same field and heating in different fields) to understand the M at low T. In these measurements, the sample was cooled from 200–10 K. At 10 K, the H was isothermally reduced to the measuring field H_{meas} and measurement is carried out while heating. We performed these measurements under two different cooling fields, i.e., $H_{cool} = 1$ T and $H_{cool} = 5$ T, Fig. 5 shows the $H_{cool} = 5$ T. For, $H_{meas=0.05T} < H_{cool}$, low T, M decreases continuously and shows a small kink at $T = 48$ K. With increasing the H_{meas}, the peak at 48 K evolves more clearly. For, $H_{meas} = H_{cool}$, at low T, M is almost constant and for $H_{meas} > H_{cool}$, at low T, M increases monotonically up to $T = 48$ K. Almost similar behavior is observed for

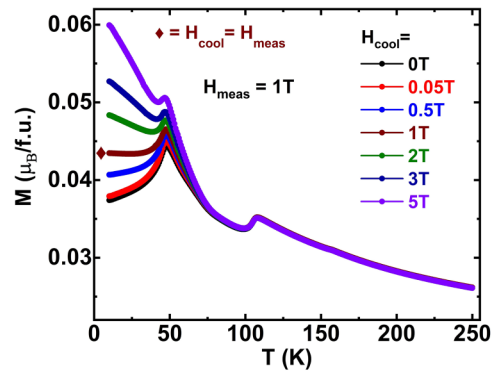

FIG. 4. M vs T curves of LBCO obtained during heating after cooling under different H.

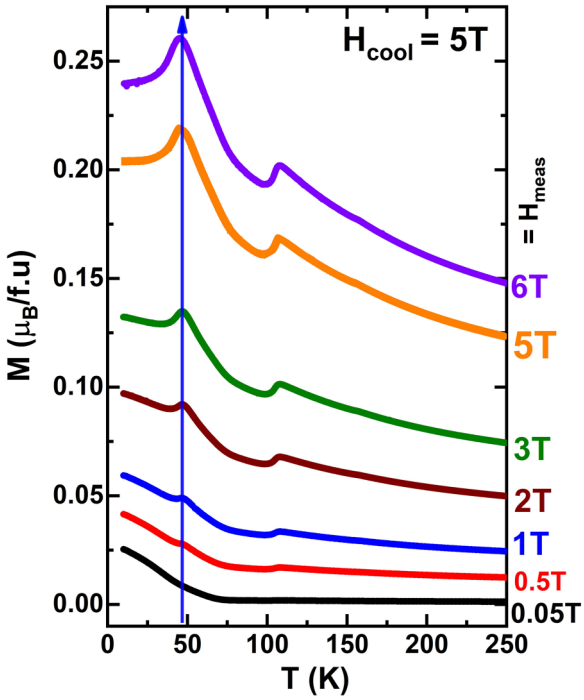

FIG. 5. M vs T curves of LBCO obtained during heating after cooling under different H.

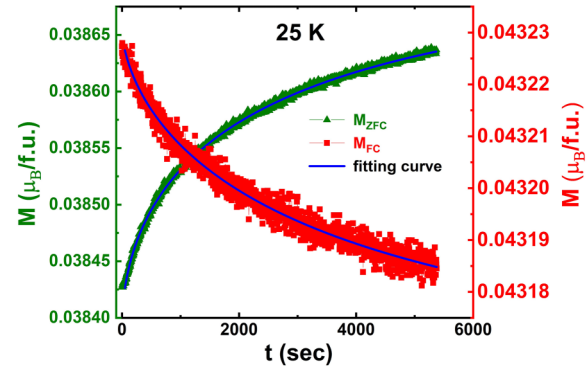

FIG. 6. Relaxation of ZFC and FC magnetization measured at $T = 25$ K. The solid lines represent the fit using a stretched exponential function in Eq. (1).

the different cooling field, i.e., H_{cool} =1 T and in this case, constant M, is evident for $H_{\text{meas}} = H_{\text{cool}}$, i.e., 1 T.

These CHUF results suggest that the low-T M is strongly dependent on the cooling and measuring fields and is almost constant for $H_{\text{meas}} = H_{\text{cool}}$. Further, from the CHUF measurements for $H_{\text{cool}} > H_{\text{meas}}$, the M at low T decreases almost linearly up to 48 K. This indicates that the frozen or arrested M (while cooling) at low T is higher and decays fast while measuring in low H_{meas}. However, for $H_{\text{cool}} < H_{\text{meas}}$, the M at low T increases up to 48 K. This behavior is similar to the ZFC in Fig. 2(a), indicating that the H_{meas} is not sufficient to de-arrest the frozen or arrested M (while cooling) at low T. Alternatively, there may be a small or negligible frozen or arrested M (while cooling) at low T. All these observations indicate that the low-T M is metastable and is kinetically arrested while cooling. Further, the kinetically arrested M state reaches a stable magnetization above 70 K. Here, we note that the de-arrest takes place at 48 K and the M, becomes stable above the 70 K.

Further, to understand the low-T magnetic state we, performed magnetic relaxation measurements at 25 K in the ZFC and FC conditions, and the obtained results are shown in Fig. 6. In the ZFC measurements, the sample was cooled from 300–5 K and at 5 K, H of 1 T was applied and the sample was heated to 25 K. After reaching 25 K, we waited for 5 min for thermal equilibrium and started measuring the M with time (t). In the FC measurements, the sample was cooled from 300–5 K, under a H of 1 T and heated from 5–25 K. After reaching 25 K, we waited for 5 min for thermal equilibrium and started measuring the M with time. From Fig. 6, it can be noted that the $M_{\text{ZFC}}(t)$ of LBCO increases from 0.03843–0.03864 $\frac{\mu_B}{f.u.}$ and the corresponding change in M is 0.54 %. However, $M_{\text{FC}}(t)$ decreases from 0.04323–0.04318 $\frac{\mu_B}{f.u.}$ and the corresponding change in M is 0.11%. At 25 K, the initial M_{FC} is 1.1 times of M_{ZFC} indicating that the M_{FC} of LBCO is closer to the equilibrium state, compared to M_{ZFC}.

In general, magnetic glassy systems are understood by analyzing their time-dependent magnetization $M(t)$, which can be expressed as [43],

$$M(t) = M_0 \pm M_g \exp\left[-\left(\frac{t}{\tau}\right)^{\beta}\right], \tag{2}$$

where, M_0 is the intrinsic M, M_g is related to a glassy component of M, τ is the characteristic relaxation time constant, and β is the stretching exponent, which has values between 0 [$M(t)$ is constant, i.e., no relaxation] and 1 [$M(t)$ relaxes with a single time constant]. In this aspect, the value of β conveys the dynamics of spins with a very strong to no relaxation limit. Further, the magnitude of β relies on the energy barriers, which are involved in the relaxation. Materials, that contain multiple energy barriers, have β values between 0 and 1, whereas for a uniform energy barrier, $\beta = 1$. The values of β obtained for the LBCO from Eq. (2) to the $M_{\text{ZFC}}(t)$ and $M_{\text{FC}}(t)$ are 0.55 and 0.62, respectively. The $\beta < 1$ values in the LBCO signify that the M relaxation evolves through multiple intermediate metastable states.

Figure 7 shows the thermal cycling of, M_{ZFC} vs T curves of LBCO measured under 1 T along with the normal ZFC, FCC, and FCW curves. In the thermal cycling of M_{ZFC} measurements, the sample was cooled from 300–10 K and at 10 K, the H of 1 T was applied. M was measured while increasing and then decreasing the T in steps of 10 K from 10–110 K. For better understanding, the M obtained from the initial thermal cycling is shown in the Fig. 7 with guided arrow marks between the T intervals of 10–30 K, and similarly the M was measured up to 110 K. In these measurements, the M value at low T increases continuously up to 60 K, and the thermal cycling between 60 K and 100 K causes the M value at low T to decrease slightly. More interestingly, the magnitude of the peak at 48 K decreases when thermal cycling is performed between 60–100 K, whereas the magnitude of the peak at 48 K increases when the thermal cycling is performed between 100 and 110 K. However, the M at low T from the thermal cycling of the $M_{\text{ZFC}}(T)$ curves does not match with the normal

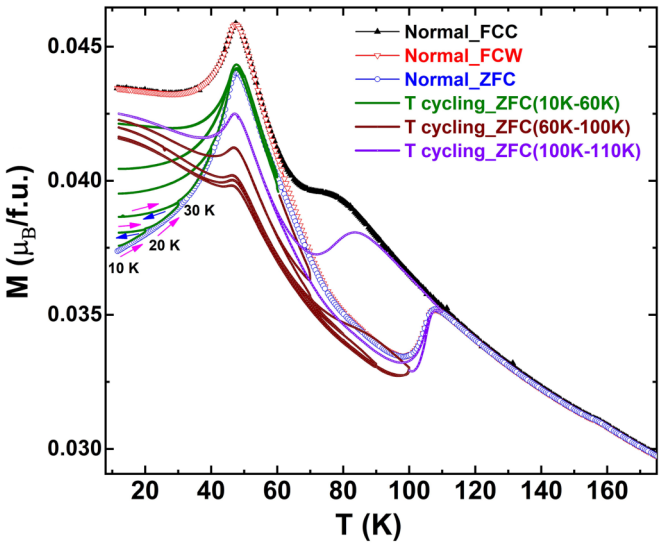

FIG. 7. Thermal cycling of M_{ZFC} vs T curves of LBCO are shown along with the normal ZFC, FCC and FCW curves measured under 1 T. The arrow marks guided the initial thermal cycling process, and the complete thermal cycling was carried out following the same procedure.

$M_{\mathrm{FCC}}(T)$ curves at the highest thermal cycling T of 110 K. The overall thermal cycling of M_{ZFC} follows the normal M_{ZFC} path and reveals that the thermal hysteresis T region plays a major role in the low-T arrested magnetic phase. These T cycling results are similar to the other magnetic glassy materials, i.e., Gd_5Ge_4 and $EuBaCo_2O_{5+\delta}$ ($\delta = 0.47$) cobaltite [34,39]. These results suggest that, at low T, even at a fixed H, thermal cycling can convert some of the supercooled metastable low-M phase (M_{ZFC}) to higher-M phase (M_{FC}) at equilibrium.

The phase coexistence at low T is further understood from the significant horizontal shift in the $M(H)$ loops measured under $\pm H$ as shown in Fig. 8. Such a shift in the $M(H)$ loop under $\pm H$ is known as exchange bias. From the shift of the $M(H)$ loops, the exchange bias field ($H_E = -[H_1 + H_2/2]$) is obtained using the H_1 (left coercive field) and H_2 (right coercive field). The H_E at 7 T in LBCO is found to be 0.46 T, which is smaller compared to the $YbBaCo_4O_7$ (YbBCO). Here, we note that YbBCO shows AFM ordering, whereas LBCO does not [30].

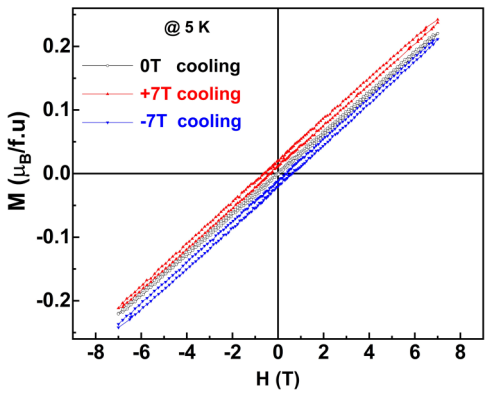

FIG. 8. Isothermal ZFC and FC, $M(H)$ loops of LBCO measured at 5 K.

IV. DIELECTRIC STUDIES

Figures 9(a) and 9(b) show the T variation of the real part of the dielectric constant (ϵ') and the corresponding loss tangent ($\tan\delta$) of the LBCO measured at different frequencies (f) with a heating rate of 2 K/min. Above 100 K the ϵ' shows a steplike increase and this behavior has also been reported in $YBaCo_4O_7$ (YBCO) and $DyBaCo_4O_7$ (DBCO) cobaltites of the same family [17], thus not shown here. For $T < 100$ K, ϵ' decreases to $T = 50$ K and starts to rise below 50 K, as shown in Fig. 9(a). At $T = 45$ K, ϵ' shows a frequency-independent peak, which is close to the magnetic peak T shown in Fig. 2(a). With a further decrease in T, ϵ' shows a broad hump centered at 20 K, where the hump is slightly dispersive with frequency; $\tan\delta$ shows frequency-independent and -dependent features below 50 K, which are shown in Fig. 9(b). The frequency-independent features at $T = 45$ K are clearly shown in the inset of Figs. 9(a) and 9(b) through the first derivative T of ϵ' and $\tan\delta$. The frequency-dependent dielectric features of LBCO are discussed later. At low T ($T < 60$ K), the magnitude of ϵ' in LBCO is in good agreement with the previously reported values of well-studied multiferroic materials in this family, such as CBCO [12,13]. The insulating nature of LBCO at low T [inset of Fig. 2(b)] and low $\tan\delta$ values below 60 K, excludes the possibility of Maxwell-Wagner-like relaxation features.

The peak at $T = 45$ K in ϵ' closely correlates with the magnetic ordering T. The structural and magnetic properties of LBCO exhibit strong sensitivity to the heating and cooling rates. Thus, we also measured the heating and cooling dependence of ϵ' and the corresponding $\frac{d\epsilon'}{dT}$ curves are shown in Fig. 9(c). Furthermore, ϵ' vs T was also measured at different heating rates, 2 K/min and 1 K/min, respectively, and the corresponding $\frac{d\epsilon'}{dT}$ curves are shown in Fig. 9(d). From, Figs. 9(c) and 9(d), it is clear that the T_{MG} and T_{DG} temperatures change significantly with the heating and cooling cycles for the same temperature sweep rate and also for the different heating rates.

The Fig. 10(a) shows the frequency variation of $\tan\delta$ at low T. The broad hump at low T in $\tan\delta$ is shifted to higher temperatures, with increasing frequency, and the corresponding maximum T of the hump (T_m) is shown in the $\frac{d\tan\delta}{dT}$ curves [Fig. 10(b)]. Figure 10(b) also shows the frequency-independent peak at 42 K. Here, we note that the $\tan\delta$ curves shown in Fig. 10(a) are measured using the homemade sample probe in a Quantum Design MPMS system and the data in Fig. 9 and Fig. 10(d) were measured using the Janis cryogenic system. Thus, there is a slight temperature difference in the T_{MG} and T_{DG}, but the overall behavior is the same. The frequency-dependent dielectric behavior at low T is analyzed using the thermally activated Arrhenius law

$$\tau = \tau_0 \exp\left(\frac{E_a}{k_B T_m}\right) \tag{3}$$

and also Vogel-Fulcher (V-F) relation [44,45],

$$\tau = \tau_0 \exp\left(\frac{E_a}{k_B (T_m - T_0)}\right). \tag{4}$$

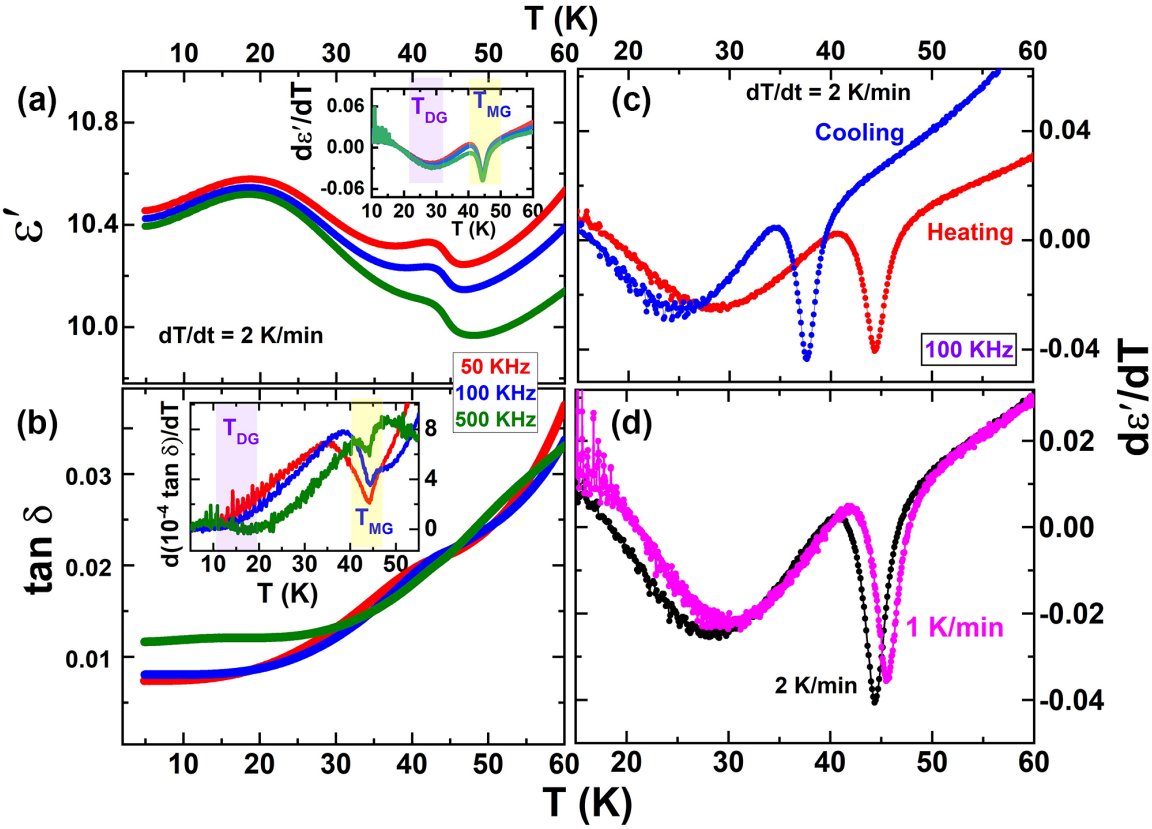

FIG. 9. The main panel of (a) and (b) shows the T variation of the ϵ' and $\tan\delta$ at different frequencies for $T < 60$ K. The inset of (a) and (b) shows the $\frac{d\epsilon'}{dT}$ and $\frac{d\tan\delta}{dT}$ curves. The various transitions are highlighted with different colors and discussed in detail in the main text. (c) shows the T variation of $\frac{d\epsilon'}{dT}$ curves measured under the same heating and cooling rates and (d) shows the $\frac{d\epsilon'}{dT}$ curves measured under different heating rates.

Here, E_a is the energy barrier to dipole reorientation, T_0 is the critical temperature at which all relaxation times diverge, τ_0 is the reciprocal of the attempt frequency (ω_0) and T_m is maximum peak temperature of ϵ'. The ϵ' vs T curves at 20 K do not follow the thermally activated Arrhenius law [the nonlinear behavior is shown in Fig. 10(c)] and also the fitting leads to a large error in τ_0. The values of the parameters E_a, τ_0, and T_0 obtained by a best-fit analysis of the data to the V-F equation are 2.78 ($\pm$0.02) meV, 2.47 ($\pm$0.61) $\times 10^{-8}s$, and 10.31 ($\pm$0.33) K, respectively.

The V-F relation is generally used to describe a glassy state in dielectrics and applies to both relaxor ferroelectric (FE) and also dipolar glass (DG) [44,45]. The relaxor FE and DG show similar broad frequency-dependent ϵ' vs T curves. However, the former can transform into normal FEs under a strong electric field (E), whereas the latter cannot. This is because relaxor FEs contain clustered polar nanoregions (PNRs), randomly interacting with individual electric dipoles of fixed length in DG [46–49]. Therefore, to distinguish the LBCO from relaxor FE and DG states, we measured (in cooling) the ϵ' vs T curves under a dc bias field (E_{bias}) of 10 kV/m. The results are shown in Fig. 10(d) along with the ϵ' vs T curves measured in the absence of E_{bias}. From, Fig. 10(d), there no obvious change in the ϵ' vs T curves under a dc bias field. Further, we have also measured the pyroelectric current at low T under an external electric field, which shows a broad pyroelectric current peak centered at 55 K. The peak position shifts along the T axis with changing heating rates. These pyroelectric results are similar to those of YBCO and DBCO cobaltites of the same family [17]; hence, they are not shown here. The pyroelectric current measurements also show the absence of permanent electric dipoles in LBCO. From these observations, we ruled out the ferroelectric (FE) and relaxor FE features in LBCO, and the low-T dielectric state is assigned to a dipolar glass.

V. DISCUSSION

The CHUF, thermal cycling of M_{ZFC}, and time-dependent M studies clearly show glasslike dynamics at low T, where the glassy phase arises from the kinetic arrest of the supercooled magnetic phase. The bulk M measurements are sufficiently sensitive to detect the phase fractions if the kinetic arrest is related to long-range magnetic order, involving the ferromagnetic and antiferromagnetic ordered phases [50]. For, LBCO, neutron studies show short-range magnetic correlations and the absence of long-range magnetic order. Thus, it is challenging to identify the phase fractions at low T in LBCO from the M studies. However, in previous x-ray, and neutron studies, along with cooling rate-dependent M studies, the M, peak at 48 K was assigned to the Cc phase [7]. At low T, in the R-114 compounds, the $Pbn2_1$ phase is more stable and exhibits AFM (or FiM) ordering, whereas the Cc phase is observed only in LBCO and is paramagnetic (PM) in nature at high T. At

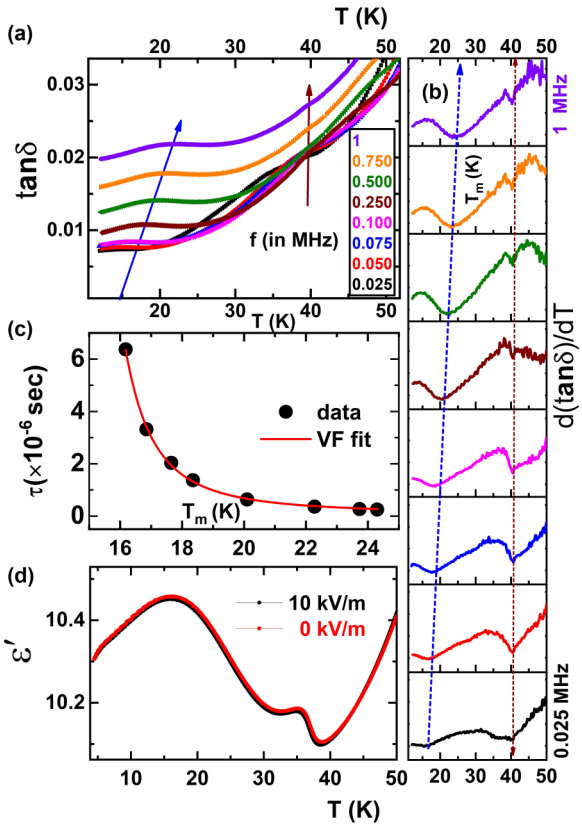

FIG. 10. (a) Low-T variation of the tan δ at different frequencies. (b) shows the frequency and temperature variation of T_m from the $\frac{d\tan\delta}{dT}$ curves. (c) shows the τ vs T_m plot along with the V-F law fitting. (d) shows the low temperature ϵ' vs T curves measured under different dc bias fields.

110 K, the Cc phase is converted to $Pbn2_1$, and at low T the phase fractions strongly depend on the cooling rates [7]. In the present experiments, we used the 3 K/min in the M studies, and 2 K/min in the ϵ' studies, which indicates LBCO contains both $Pbn2_1$, Cc phases qualitatively. However, as indicated above, the exact phase fractions cannot be predicted. If the high-T PM Cc phase is kinetically arrested at low T, without showing any long-range magnetic order, then one would expect the M associated with this phase to decrease linearly without showing any peak, i.e., pure PM behavior. On the other hand, the M investigations clearly display an AFM-like peak at 48 K suggesting that the $Pbn2_1$ phase fraction contributes significantly to the kinetic arrest and might be produce a peak at 48 K, during heating. This can be further understood from the thermal cycling of $M_{\rm ZFC}$ (Fig. 7), where the peak at 48 K, becomes weak when we perform the T cycling in 60–100 K and also at the low T, M shows linear decrease. We note that in the thermal cycling of $M_{\rm ZFC}$, a heating and cooling rate of 3 K/min was used and it was observed that the $M_{\rm ZFC}$ peak at 48 K becomes weaker. A similar behavior is also reported in Ref. [7], where the M was measured using slower cooling rates (<1 K/min).

We now present additional evidence suggesting that the peak near 48 K might be associated with the $Pbn2_1$ phase by comparing the ϵ' properties of LBCO with the reported ϵ' studies of other R-114 cobaltites. The crystal structure of CBCO is orthorhombic $Pbn2_1$ (300–4 K; noncentrosymmetric) and exhibits long-range FiM ordering at low T ($T_c \approx 60$ K). The ϵ' studies on CBCO at low T show a frequency-independent peak at magnetic ordering T. For $T < T_c$, ϵ' of CBCO decreases with decreasing T, without showing any relaxation features [9,12–14]. However, the dielectric studies on the YBCO and DBCO cobaltites show the absence of the ϵ' peak at low T and is also constant for $T < 30$ K [17]. Here, we note that the magnetic ground states of these YBCO and DBCO cobaltites are different, DBCO shows spin glasslike behavior along with short-range magnetic correlations, whereas YBCO shows both long-range and short-range magnetic features below 100 K [17–19]. Based on these ϵ' comparisons, we attribute the frequency-independent peak of LBCO at $T = 45$ K to the $Pbn2_1$ phase. Further, as discussed above, the kinetically arrested PM Cc phase at low T in LBCO would likely show dipolar glassy features in the dielectric studies.

VI. CONCLUSION

In conclusion, we report experimental evidence of magnetic and dielectric glassy states in alternating kagome and triangular lattice $LuBaCo_4O_7$ cobaltite. ac magnetization studies show an absence of the conventional spin glass state, whereas various detailed dc M studies show the magnetic glassy state at low T, arising from the kinetic arrest of the first-order structural phases. Thermal cycling measurements show that broad thermal hysteresis plays a significant role on the arrested low-T magnetic phases. The dielectric features of the LBCO are strongly coupled with the magnetic phase transition and also show strong signatures of kinetically arrested phases. Recent studies have established that phase fractions at low temperature in LBCO vary significantly with Y doping at Lu sites [51]. Thus, studying $Lu_{1-x}Y_xBaCo_4O_7$, systematically may shed more light on the origin of the kinetic arrest-driven magnetic and dielectric glassy features and the role of phase coexistence in these systems.

ACKNOWLEDGMENTS

This work is funded by the Science and Engineering Research Board (SERB) under the National Post-Doctoral Fellowship (NPDF/2021/002536), India. This study is supported by the National Science and Technology Council, Taiwan, under Grants No. NSTC-112-2112-M-110-018, No. NSTC-113-2112-M-110-006, and No. NSTC-114-2811-M-110 -001-NSTC-113-2112-M-110 -018 -MY2. The author group from IIT Bombay acknowledges the support of central measurement facilities (HR-XRD, SQUID MPMS) at their institution. The authors of IIT Kharagpur acknowledge the support of central SQUID magnetometer facilities.

DATA AVAILABILITY

The data supporting this study's findings are available within the article.

[1] A. Maignan, V. Caignaert, D. Pelloquin, S. Hébert, V. Pralong, J. Hejtmanek, and D. Khomskii, Spin, charge, and lattice coupling in triangular and kagomé sublattices of CoO_4 tetrahedra : $YbBaCo_4O_{7+\delta}$ (δ= 0, 1), Phys. Rev. B **74**, 165110 (2006).

[2] V. Kocsis, Y. Tokunaga, T. Rõom, U. Nagel, J. Fujioka, Y. Taguchi, Y. Tokura, and S. Bordács, Spin-lattice and magnetoelectric couplings enhanced by orbital degrees of freedom in polar multiferroic semiconductors, Phys. Rev. Lett. **130**, 036801 (2023).

[3] E. A. Juarez-Arellano, A. Friedrich, D. J. Wilson, L. Wiehl, W. Morgenroth, B. Winkler, M. Avdeev, R. B. Macquart, and C. D. Ling, Single-crystal structure of $HoBaCo_4O_7$ at ambient conditions, at low temperature, and at high pressure, Phys. Rev. B **79**, 064109 (2009).

[4] T. Sarkar, V. Caignaert, V. Pralong, and B. Raveau, Hysteretic magnetictransportstructural transition in 114 cobaltites: Size mismatch effect, Chem. Mater. **22**, 6467 (2010).

[5] B. Raveau and M. Seikh, *Cobalt Oxides: From Crystal Chemistry to Physics* (John Wiley & Sons, New York, 2012).

[6] V. Caignaert, V. Pralong, V. Hardy, C. Ritter, and B. Raveau, Magnetic structure of $CaBaCo_4O_7$: Lifting of geometrical frustration towards ferrimagnetism, Phys. Rev. B **81**, 094417 (2010).

[7] S. Avci, O. Chmaissem, H. Zheng, A. Huq, D. D. Khalyavin, P. W. Stephens, M. R. Suchomel, P. Manuel, and J. F. Mitchell, Kinetic control of structural and magnetic states in $LuBaCo_4O_7$, Phys. Rev. B **85**, 094414 (2012).

[8] Z. A. Kazei, V. V. Snegirev, A. S. Andreenko, and L. P. Kozeeva, Anomalies in the Young modulus at structural phase transitions in rare-earth cobaltites $RBaCo_4O_7$ (R = Y,Tm-Lu), J. Exp. Theor. Phys. **113**, 245 (2011).

[9] V. Caignaert, A. Maignan, K. Singh, C. Simon, V. Pralong, B. Raveau, J. F. Mitchell, H. Zheng, A. Huq, and L. C. Chapon, Gigantic magnetic-field-induced polarization and magnetoelectric coupling in a ferrimagnetic oxide $CaBaCo_4O_7$, Phys. Rev. B **88**, 174403 (2013).

[10] N. Hollmann, Z. Hu, M. Valldor, A. Maignan, A. Tanaka, H. H. Hsieh, H.-J. Lin, C. T. Chen, and L. H. Tjeng, Electronic and magnetic properties of the kagome systems $YBaCo_4O_7$ and $YBaCo_3MO_7$ (M = Al,Fe), Phys. Rev. B **80**, 085111 (2009).

[11] D. D. Khalyavin, L. C. Chapon, P. G. Radaelli, H. Zheng, and J. F. Mitchell, Structural behavior of the kagome antiferromagnet $TmBaCo_4O_7$: Neutron diffraction study and group-theoretical consideration, Phys. Rev. B **80**, 144107 (2009).

[12] K. Singh, V. Caignaert, L. C. Chapon, V. Pralong, B. Raveau, and A. Maignan, Spin-assisted ferroelectricity in ferrimagnetic $CaBaCo_4O_7$, Phys. Rev. B **86**, 024410 (2012).

[13] C. Dhanasekhar, A. K. Das, R. Singh, A. Das, G. Giovannetti, D. Khomskii, and A. Venimadhav, Switching from pyroelectric to ferroelectric order in Ni-doped $CaBaCo_4O_7$, Phys. Rev. B **96**, 134413 (2017).

[14] C. Dhanasekhar, A. Das, and A. Venimadhav, Multiple caloric effects in geometrically frustrated "114" $CaBaCo_4O_7$ cobaltite, J. Magn. Magn. Mater. **418**, 76 (2016).

[15] M. Ruan, Z. Ouyang, Y. Guo, Y. Sun, J. Cheng, Z. Xia, and G. Rao, Spin-glass-like freezing in geometrically frustrated compound $InBaCo_4O_7$, Solid State Sci. **45**, 1 (2015).

[16] J. Kumar, S. N. Panja, S. Dengre, and S. Nair, Identification of a griffiths singularity in a geometrically frustrated antiferromagnet, Phys. Rev. B **95**, 054401 (2017).

[17] C. Dhanasekhar, A. K. Das, A. Das, S. K. Mishra, R. Rawat, and A. Venimadhav, Structural, magnetic and electric-polarization properties of geometrically frustrated $YBaCo_4O_7$ and $DyBaCo_4O_7$cobaltites, Europhys. Lett. **127**, 67001 (2019).

[18] P. Manuel, L. C. Chapon, P. G. Radaelli, H. Zheng, and J. F. Mitchell, Magnetic correlations in the extended kagome $YBaCo_4O_7$probed by single-crystal neutron scattering, Phys. Rev. Lett. **103**, 037202 (2009).

[19] D. D. Khalyavin, P. Manuel, B. Ouladdiaf, A. Huq, P. W. Stephens, H. Zheng, J. F. Mitchell, and L. C. Chapon, Publisher's note: Spin-ordering and magnetoelastic coupling in the extended kagome system $YBaCo_4O_7$, Phys. Rev. B **85**, 059903(E) (2012).

[20] W. Schweika, M. Valldor, J. D. Reim, and U. K. Rößler, Chiral spin liquid ground state in $YBaCo_3FeO_7$, Phys. Rev. X **12**, 021029 (2022).

[21] A. Bludov, S. Gnatchenko, R. Szymczak, H. Szymczak, S. Barilo, G. Bychkov, and S. Shiryaev, A magnetic-field-induced irreversible transition in geometrically frustrated antiferromagnetic $TbBaCo_4O_7$ with kagome and triangular lattices, Low Temp. Phys. **35**, 971 (2009).

[22] R. Szymczak, A. N. Bludov, S. L. Gnatchenko, S. N. Barilo, A. Jezierski, and H. Szymczak, Field-induced magnetic order in frustrated $TbBaCo_4O_7$ single crystals, Acta Phys. Pol. A **118**, 299 (2010).

[23] M. M. Seikh, T. Sarkar, V. Pralong, V. Caignaert, and B. Raveau, Dramatic effect of a-site substitution upon the structure and magnetism of the "114" $CaBaCo_4O_7$ cobaltite, Phys. Rev. B **86**, 184403 (2012).

[24] C. Dhanasekhar, A. K. Das, A. Das, and A. Venimadhav, Ferroelectricity in $CaBaCo_4O_7$ by light non magnetic Zn, J. Phys.: Condens. Matter **32**, 385802 (2020).

[25] M. Soda, T. Moyoshi, Y. Yasui, M. Sato, and K. Kakurai, Successive phase transitions of $LuBaCo_4O_7$ with kagome and triangular lattices, J. Phys. Soc. Jpn. **76**, 084701 (2007).

[26] M. Soda, K. Morita, G. Ehlers, F. Ye, T. Tohyama, H. Yoshizawa, T. Masuda, and H. Kawano-Furukawa, Magnetic diffuse scattering of $YBaCo_4O_7$ and $LuBaCo_4O_7$ on kagome and triangular lattices, J. Phys. Soc. Jpn. **90**, 074704 (2021).

[27] A. Tiwari, D. C. Kakarla, M.-J. Hsieh, J.-Y. Lin, C. W. Wang, L. K. Tseng, C. E. Lu, A. Pal, T. W. Kuo, M. M. C. Chou, and H. D. Yang, Observation of magnetic field-induced second magnetic ordering and peculiar ferroelectric polarization in L - type ferrimagnetic $Fe_2(MoO_4)_3$, Phys. Rev. Mater. **6**, 094412 (2022).

[28] A. Pal, T. W. Yen, T. W. Kuo, C. W. Wang, S. M. Huang, M. C. Chou, Y. C. Lai, Y. C. Chuang, P. Yanda, A. Sundaresan, H. S. Kunwar, V. G. Sathe, A. Tiwari, D. C. Kakarla, and H. D. Yang, Unconventional multiferroicity induced by structural distortion and magnetostriction effect in the layered spin-1/2 ferrimagnet $Bi_2Cu_5B_5O_{14}$, Phys. Rev. B **107**, 184430 (2023).

[29] L. C. Chapon, P. G. Radaelli, H. Zheng, and J. F. Mitchell, Competing magnetic interactions in the extended kagomé system $YBaCo_4O_7$, Phys. Rev. B **74**, 172401 (2006).

[30] K. Dey, S. Majumdar, and S. Giri, Giant exchange bias effect with low-coercivity in $YbBaCo_4O_7$, J. Alloys Compd. **753**, 329 (2018).

[31] K. Jonason, E. Vincent, J. Hammann, J. P. Bouchaud, and P. Nordblad, Memory and chaos effects in spin glasses, Phys. Rev. Lett. **81**, 3243 (1998).

[32] J. Krishna Murthy and A. Venimadhav, Giant zero field cooled spontaneous exchange bias effect in phase separated $La_{1.5}Sr_{0.5}CoMnO_6$, Appl. Phys. Lett. **103**, 252410 (2013).

[33] S. Kundu, T. Dey, A. V. Mahajan, and N. Büttgen, $LiZn_2V_3O_7$: a new geometrically frustrated cluster spin-glass, J. Phys.: Condens. Matter **32**, 115601 (2020).

[34] A. Kumari, C. Dhanasekhar, P. Chaddah, D. C. Kakarla, H. D. Yang, Z. H. Yang, B. H. Chen, Y. C. Chung, and A. K. Das, Magnetic glassy state at low spin state of Co^{3+} in $EuBaCo_2O_{5+\delta}$ ($\delta = 0.47$) cobaltite, J. Phys.: Condens. Matter **32**, 155803 (2020).

[35] A. Banerjee, K. Kumar, and P. Chaddah, Enhancement of equilibrium fraction in $La_{0.5}Ca_{0.5}MnO_3$ by recrystallization, J. Phys.: Condens. Matter **20**, 255245 (2008).

[36] A. Banerjee, K. Kumar, and P. Chaddah, Conversion of a glassy antiferromagnetic-insulating phase to an equilibrium ferromagnetic-metallic phase by devitrification and recrystallization in Al substituted $Pr_{0.5}Ca_{0.5}MnO_3$, J. Phys.: Condens. Matter **21**, 026002 (2009).

[37] X. F. Miao, Y. Mitsui, A. I. Dugulan, L. Caron, N. V. Thang, P. Manuel, K. Koyama, K. Takahashi, N. H. van Dijk, and E. Brück, Kinetic-arrest-induced phase coexistence and metastability in $(Mn, Fe)_2(P, Si)$, Phys. Rev. B **94**, 094426 (2016).

[38] S. B. Roy and M. K. Chattopadhyay, Contrasting the magnetic response between a magnetic glass and a reentrant spin glass, Phys. Rev. B **79**, 052407 (2009).

[39] S. B. Roy, M. K. Chattopadhyay, P. Chaddah, J. D. Moore, G. K. Perkins, L. F. Cohen, K. A. Gschneidner, and V. K. Pecharsky, Evidence of a magnetic glass state in the magnetocaloric material Gd_5Ge_5, Phys. Rev. B **74**, 012403 (2006).

[40] S. Roy and P. Chaddah, Phase-coexistence and glass-like behavior in magnetic and dielectric solids with long-range order, Phys. Status Solidi B **251**, 2010 (2014).

[41] M. K. Chattopadhyay, S. B. Roy, and P. Chaddah, Kinetic arrest of the first-order ferromagnetic-to-antiferromagnetic transition in $Ce(Fe_{0.96}Ru_{0.04})_2$: Formation of a magnetic glass, Phys. Rev. B **72**, 180401(R) (2005).

[42] W. Wu, C. Israel, N. Hur, S. Park, S.-W. Cheong, and A. De Lozanne, Magnetic imaging of a supercooling glass transition in a weakly disordered ferromagnet, Nat. Mater. **5**, 881 (2006).

[43] P. Bag, P. R. Baral, and R. Nath, Cluster spin-glass behavior and memory effect in $Cr_{0.5}Fe_{0.5}Ga$, Phys. Rev. B **98**, 144436 (2018).

[44] G. A. Samara, The relaxational properties of compositionally disordered ABO_3 perovskites, J. Phys.: Condens. Matter **15**, R367 (2003).

[45] J. Yang, W. Bai, Y. Zhang, C. gang Duan, J. Chu, and X. Tang, Dielectric phenomena of multiferroic oxides at acoustic- and radio-frequency, J. Phys.: Condens. Matter **35**, 463001 (2023).

[46] R. Pirc and Z. Kutnjak, Electric-field dependent freezing in relaxor ferroelectrics, Phys. Rev. B **89**, 184110 (2014).

[47] V. Polinger and I. B. Bersuker, Origin of polar nanoregions and relaxor properties of ferroelectrics, Phys. Rev. B **98**, 214102 (2018).

[48] L. Yin, R. Zhang, J. Yang, P. Tong, W. Song, J. Dai, X. Zhu, and Y. Sun, Quantum paraelectricity to dipolar glass transition in Sc doped $BaFe_{12}O_{19}$ single crystals, Appl. Phys. Lett. **115**, 262902 (2019).

[49] C. Filipič, Z. Kutnjak, R. Pirc, G. Canu, and J. Petzelt, $BaZr_{0.5}Ti_{0.5}O_3$: Lead-free relaxor ferroelectric or dipolar glass, Phys. Rev. B **93**, 224105 (2016).

[50] S. Pal, K. Kumar, and A. Banerjee, Phase coexistence and nonequilibrium dynamics under simultaneously applied magnetic field and pressure: Possible role of the interface, Phys. Rev. B **108**, 214409 (2023).

[51] S. Sahinbay, H. Zheng, J. F. Mitchell, S. Rosenkranz, and O. Chmaissem, Frustration-mediated crossover from long-range to short-range magnetic ordering in $Y_{1-X}Lu_XBaCo_4O_7$, Phys. Rev. B **110**, 014438 (2024).